Nanoscale Res Lett (2009) 4:491–497
DOI 10.1007/s11671-009-9266-1

NANO EXPRESS

# Low Temperature Growth of $In_2O_3$ and InN Nanocrystals on Si(111) via Chemical Vapour Deposition Based on the Sublimation of $NH_4Cl$ in In

**Matthew Zervos · Demetra Tsokkou · Maria Pervolaraki · Andreas Othonos**

Received: 30 November 2008 / Accepted: 27 January 2009 / Published online: 21 February 2009
© to the authors 2009

**Abstract** Indium oxide ($In_2O_3$) nanocrystals (NCs) have been obtained via atmospheric pressure, chemical vapour deposition (APCVD) on Si(111) via the direct oxidation of In with Ar:10% $O_2$ at 1000 °C but also at temperatures as low as 500 °C by the sublimation of ammonium chloride ($NH_4Cl$) which is incorporated into the In under a gas flow of nitrogen ($N_2$). Similarly InN NCs have also been obtained using sublimation of $NH_4Cl$ in a gas flow of $NH_3$. During oxidation of In under a flow of $O_2$ the transfer of In into the gas stream is inhibited by the formation of $In_2O_3$ around the In powder which breaks up only at high temperatures, i.e. $T > 900$ °C, thereby releasing In into the gas stream which can then react with $O_2$ leading to a high yield formation of isolated 500 nm $In_2O_3$ octahedrons but also chains of these nanostructures. No such NCs were obtained by direct oxidation for $T_G < 900$ °C. The incorporation of $NH_4Cl$ in the In leads to the sublimation of $NH_4Cl$ into $NH_3$ and HCl at around 338 °C which in turn produces an efficient dispersion and transfer of the whole In into the gas stream of $N_2$ where it reacts with HCl forming primarily InCl. The latter adsorbs onto the Si(111) where it reacts with $H_2O$ and $O_2$ leading to the formation of $In_2O_3$ nanopyramids on Si(111). The rest of the InCl is carried downstream, where it solidifies at lower temperatures, and rapidly breaks down into metallic In upon exposure to $H_2O$ in the air. Upon carrying out the reaction of In with $NH_4Cl$ at 600 °C under $NH_3$ as opposed to $N_2$, we obtain InN nanoparticles on Si(111) with an average diameter of 300 nm.

**Keywords** Indium oxide · Indium nitride · Nanocrystals · Low temperature · Chemical vapour deposition

One of the fundamental building blocks necessary for the development of nanotechnology are semiconductor nanodots (NDs), nanocrystals (NCs) or nanoparticles (NPs) viz. quantum dots (QDs). These are completely quantised, zero dimensional (0D) semiconductors with discrete energy levels whose electronic and optoelectronic properties are size dependent. Semiconductor QDs have been traditionally obtained by strained layer growth using molecular beam epitaxy (MBE) or chemical vapour deposition (CVD) [1, 2]. However, during recent years NDs, NCs and NPs have also been obtained using complex chemical synthesis involving solid, liquid and gas reactions and a broad variety of methods including hydrothermal and colloidal synthesis. So far, NDs, NCs, NPs have been realised from group IV elemental semiconductors like Si [3, 4] and Ge [5] but also III-V and II-VI compound semiconductors like GaAs [6], InP [7, 8], InN [9] GaN [10], ZnS [11, 12], CdS [13] and oxides like ZnO [14–17], $SnO_2$ [18] and $In_2O_3$ [19–28]. Among the III-V's, nitride (N) semiconductors are especially attractive due to the fact that their energy band gap can be adjusted over a very wide range e.g. between 0.7 eV for InN up to 3.4 eV in GaN by changing the composition of the ternary semiconductor $In_xGa_{1-x}N$ over $0 \leq x \leq 1$. On the other hand, among the oxides, $In_2O_3$ is a very important wide-band gap semiconductor ($E_G = 3.55$ eV) which is widely used for the fabrication of devices such as electro-optic modulators, solar cells, electro-chromic mirrors and sensors [29].

M. Zervos (✉) · M. Pervolaraki
Department of Mechanical and Manufacturing Engineering, Materials Science Group, Nanostructured Materials and Devices Laboratory, University of Cyprus, P.O. Box 20537, 1678 Nicosia, Cyprus
e-mail: zervos@ucy.ac.cy

D. Tsokkou · A. Othonos
Department of Physics, Research Centre of Ultrafast Science, University of Cyprus, P.O. Box 20537, 1678 Nicosia, Cyprus

To date $In_2O_3$ NCs have been obtained via CVD using $In_2O_3$:In in a flow of Ar:$CH_4$ at 950 °C by Jia et al. [19] or just Ar between 950 and 1300 °C by Cheng et al. [20] and Guha et al. [21]. Similarly, chains of $In_2O_3$ NCs have been obtained by direct oxidation of In which was heated to 900 °C [25]. High yields are critical in order to successfully fabricate nano-devices and low temperatures desirable for compatibility with mainstream silicon processes but also those involving polymers. One of the shortcomings in the synthesis of $In_2O_3$ nanostructures obtained by CVD is the fact that until now high temperatures have been used. Low temperature synthesis of $In_2O_3$ NPs has been demonstrated via the sol–gel method by Zhou et al. [22], which took, however, >100 h and involved annealing between 500 and 850 °C. In addition, a high yield-low temperature synthesis of single crystalline tin doped indium oxide octahedrons via a low temperature, catalyst-free process was also demonstrated by Wei et al. [23], who obtained nanostructures as low as 450 °C using a solution of indium acetate and tin chloride. Therefore, there is active interest in the low temperature synthesis of $In_2O_3$ NCs and an active, growing interest in InN QDs which have been grown by MBE or metal organic CVD (MOCVD) predominantly on GaN, AlN, $Al_2O_3$. Very few investigations have been carried out on the synthesis of colloidal InN NPs [9] while recently indium oxynitride which can be thought of as an alloy between InN and $In_2O_3$ was investigated and proposed for optoelectronic device applications [30].

In this work, we have investigated the synthesis of $In_2O_3$ NCs by direct oxidation of In with $O_2$ in an atmospheric pressure (APCVD) reactor and the limitations that arise as a consequence of the direct oxidation process. We find that during direct oxidation of In by $O_2$ the transfer of In into the gas stream is inhibited by the formation of an $In_2O_3$ shell around the In powder which melts at 157 °C. The $In_2O_3$ shell breaks up only at high growth temperatures ($T_G$) i.e. $T_G > 900$ °C, thereby releasing In into the gas stream which in turn reacts with $O_2$ leading to the formation of a high yield of $In_2O_3$ octahedrons with sizes of 500 nm but also chains of these nanostuctures. No such nanostructures were obtained by direct oxidation for $T < 900$ °C. We find that including $NH_4Cl$ into the In under a gas flow of $N_2$ leads to the sublimation of $NH_4Cl$ into $NH_3$ and HCl at around 338 °C which results into the complete transfer of the In precursor into the gas stream of $N_2$ where it reacts with HCl and forms InCl that adsorbs onto the Si(111) and reacts with $H_2O$ and $O_2$ forming $In_2O_3$ nanopyramids at temperatures as low as 500 °C. Upon carrying out the reaction under $NH_3$ as opposed to $N_2$ we obtain InN nanoparticles with an average diameter of 300 nm. The low temperature growth of InN and $In_2O_3$ NCs directly on Si(111) using a common type of reaction could be exploited for the synthesis of InN/$In_2O_3$ heteronanostructures for a diverse range of applications such as solar cells, sensors, etc.

## Experimental

The In-based nanostructures were grown using an APCVD reactor which consists of four mass flow controllers (MFC's) and a horizontal quartz tube furnace, capable of reaching a maximum temperature of 1100 °C. More specifically, we used $n^+$ Si(111) and $n^+$ Si(111) covered with a thin layer of Au that had a thickness of a few nm's. The Si(111) samples had an area of $\approx 1$ cm$^2$ and initially they were immersed in HF, rinsed in de-ionised water and dried with nitrogen prior to the deposition of the Au layer in order to remove the native oxide and surface contamination. The Au layer was deposited via sputtering at a rate of 0.1 nm/s using an Ar plasma under a pressure $<10^{-4}$ mBar. For the purpose of optical measurements all of the In-based NCs were grown directly on quartz.

In the case of direct oxidation at high temperatures, fine In powder (Aldrich, Mesh-100, 99.99%) was weighed and loaded into a quartz boat together with a Au/Si(111) and plain Si(111) sample. The Au/Si(111) sample was positioned about 5 mm over the In and the Si(111) about 10 mm downstream from the In powder. Then the boat was loaded into the quartz tube reactor and positioned directly above the thermocouple used to measure the heater temperature at the centre of tube. After loading the boat at room temperature (RT), Ar (99.999%) was introduced at a flow rate of 500 standard cubic centimetres per minute (sccm) for 10 min, in order to purge the tube. Following this, the temperature was ramped to the desired growth temperature ($T_G$) in a reduced Ar flow of 100 sccm. Upon reaching $T_G$ the flow of Ar was reduced to 90 sccm and $O_2$ introduced at a flow of 10 sccm for another 60 min after which the $O_2$ flow was cut off and the quartz tube was allowed to cool down over at least 60 min in an inert gas flow of Ar, 100 sccm. The sample was removed only when the temperature was lower than 100 °C.

For the synthesis of $In_2O_3$ NCs at low temperatures, an equimolar mixture of In powder (Aldrich, Mesh-100, 99.99%) and $NH_4Cl$ (99%, VWR) was prepared and loaded in the centre of the quartz boat. A Au/Si(111) sample was positioned over the mixture of In and $NH_4Cl$ and a Si(111) sample without Au downstream from the mixture as described above. After loading the boat at room temperature (RT), nitrogen $N_2$ (99.999%) was introduced at a flow rate of 500 sccm for 15 min in order to purge the tube. Following this, the temperature was ramped to the desired growth temperature ($T_G$) in a $N_2$ flow of 100 sccm's. Upon reaching $T_G$ the flow of $N_2$ was maintained at 100 sccm for

a further 60 min after which the quartz tube was allowed to cool down over at least 60 min. Finally the InN NCs were obtained by using an equimolar mixture of In:$NH_4Cl$ and exactly the same growth conditions that led to the formation of InN nanowires by direct nitridation of In at 600 °C under a gas flow of 250 sccm $NH_3$ which is described in detail elsewhere [31].

The morphology of the nanostructures were examined with a TESCAN scanning electron microscope (SEM) and the crystal structure and phase purity of the nanostructures were investigated using a SHIMADZU, XRD-6000, X-ray diffractometer and Cu, Ka source. A scan of $\theta$–$2\theta$ in the range between 10° and 80° was performed for the nanostructures grown under different conditions. For the XRD we used Al and stainless steel ($Fe_3C$) holders to place the samples on the goniometer. In some of the XRD patterns the characteristic peaks of the holder material were detected and identified. Finally, optical spectroscopy was carried out using a standard spectrophotometer UV/V (Perkin Elmer Lambda 950) in the reflection mode at near normal incident to minimise scattering effects from the sample.

## Results

In the case of direct oxidation of In with $O_2$ we observed the formation of $In_2O_3$ NCs only for $T_G \geq 900$ °C and a typical SEM image of $In_2O_3$ NCs grown at $T_G = 1000$ °C is shown in Fig. 1a. Following the reaction we found that the In powder had expanded significantly into a porous like solid which disintegrated easily into a powder while a bright yellow dust corresponding to the $In_2O_3$ NCs was found on the Si(111) but also in plentiful supply on the sides of the quartz tube. The $In_2O_3$ NCs are octahedrons and had the tendency to form large dendrites consisting of $In_2O_3$ NC chains as shown in Fig. 1b and c, respectively. The small $In_2O_3$ NCs have a diameter of $\approx$500 nm, while the sizes of the larger octahedrons are almost $\approx$2500 nm.

The surface density of the $In_2O_3$ NCs across the surface of the Si(111) was very uniform and the density of the dendrites was dependent on the amount of In and the distance of the silicon from the In. The $In_2O_3$ NCs grown at $T_G = 1000$ °C on silicon exhibited clear peaks in the X-ray diffraction spectra shown in Fig. 2 and have a cubic structure, while the optical bandgap is near 3.5 eV as determined from the reflection spectrum shown in Fig. 3.

As already stated above, no nanostructures were obtained for $T_G < 900$ °C in the presence of $O_2$ and the In powder which melts at 157 °C forms a well-defined sphere in the quartz boat found after each growth run. The surface of the In had a grey, non-reflective appearance as opposed

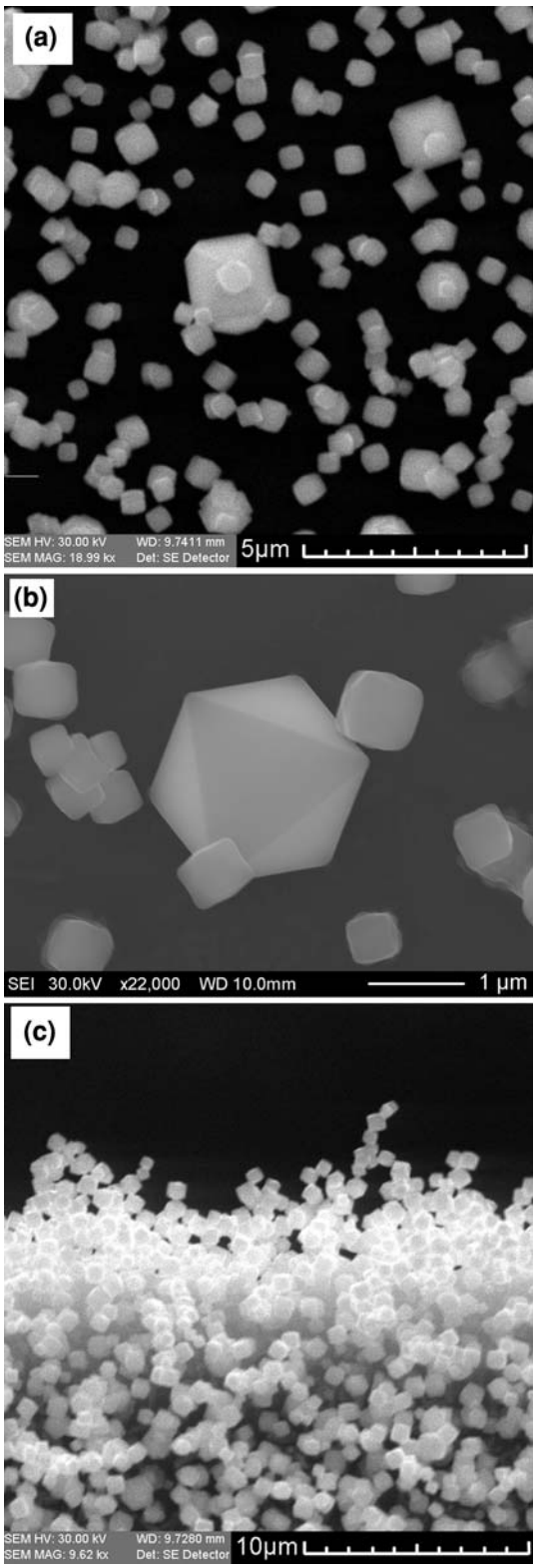


**Fig. 1** $In_2O_3$ NCs grown on Si(111) by direct oxidation of In with $O_2$ at 1000 °C (**a**) Isolated NCs with min diameter of 500 nm (**b**) Dendrite structure consisting of chains of NCs (**c**) Side view of NC chains

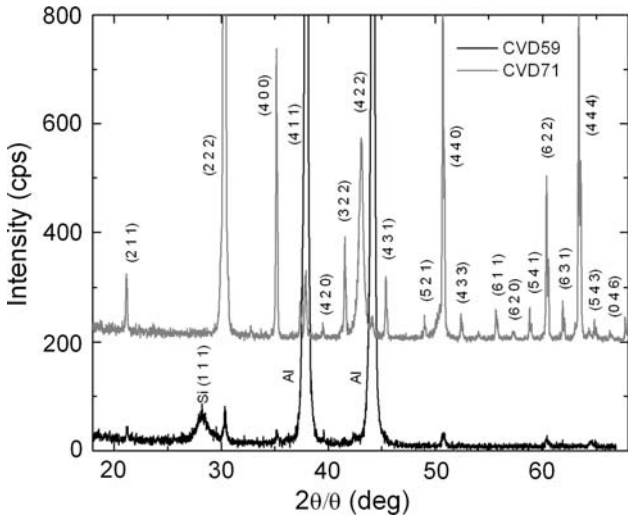


**Fig. 2** XRD spectrum of $In_2O_3$ NCs grown on Si(111) (i) by direct oxidation of In by Ar:10% $O_2$ at 1000 °C, i.e. CVD71, top pattern and (ii) by reaction of In with $NH_4Cl$ at 600 °C under a flow of $N_2$ i.e. CVD59, lower pattern. Enhanced $In_2O_3$ peaks are obtained from the sample grown at the higher temperature

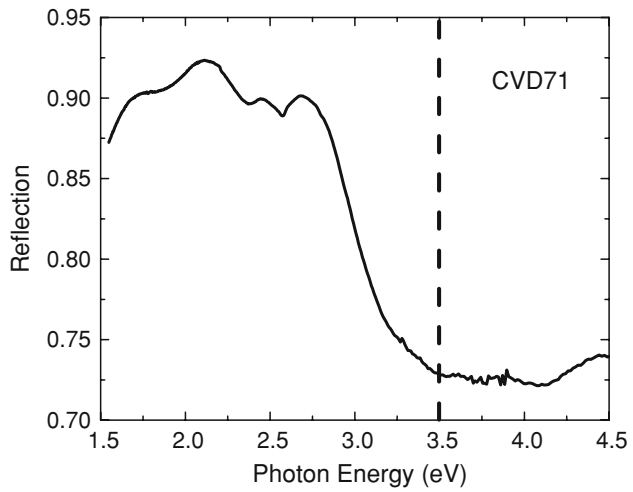


**Fig. 3** Reflection spectrum of the $In_2O_3$ NCs grown at 1000 °C directly on quartz

to the highly reflective surface of In which we always obtained during the growth of InN from In and $NH_3$ [31].

In contrast to the above findings, the reaction of In and $NH_4Cl$ occurred efficiently even at temperatures as low as 400 °C, since no trace of the In:$NH_4Cl$ mixture whatsoever was found in the boat after removing the latter from the quartz tube. In addition, a dark yellow powder was always found near the cool end of the reactor which rapidly turned into metallic grey upon exposure to the ambient air.

A typical SEM image of $In_2O_3$ NCs obtained on Si(111) at 600 °C after the reaction of In with $NH_4Cl$ under $N_2$ is shown in Fig. 4a. Larger $In_2O_3$ NCs were obtained at $T_G = 500$ °C, as shown in Fig. 4b. Interestingly, no

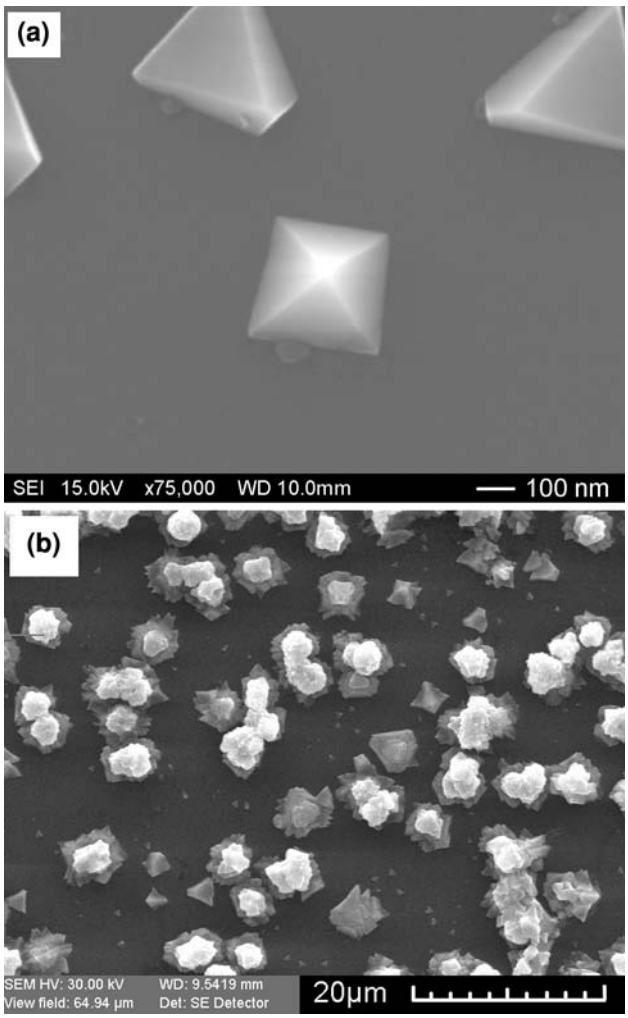


**Fig. 4** (**a**) $In_2O_3$ NCs as small as 200 nm were grown on Si(111) at 600 °C via the reaction of In and $NH_4Cl$. The large pyramids have a base almost equal to 2000 nm (**b**) Coalescence of $In_2O_3$ NCs into small flower like structures at 500 °C

nano-pyramids were obtained on the Si(111) that was covered with a few nm's of Au and positioned directly over the In:$NH_4Cl$ mixture.

## Discussion

To date $In_2O_3$ NCs have been obtained using CVD either by direct oxidation of In or by reduction of $In_2O_3$ at high temperatures [19–21]. In the case of direct oxidation of In with $O_2$ a shell of $In_2O_3$ forms around the molten source of In. This shell inhibits the transfer of In into the gas stream, so it is necessary to increase the temperature above 900 °C in order to break the shell and ensure an adequate transfer of In into the gas stream. This leads to an apparent expansion of the In very similar to that which occurs during the nitridation of Al when it reacts with $NH_3$. In the latter

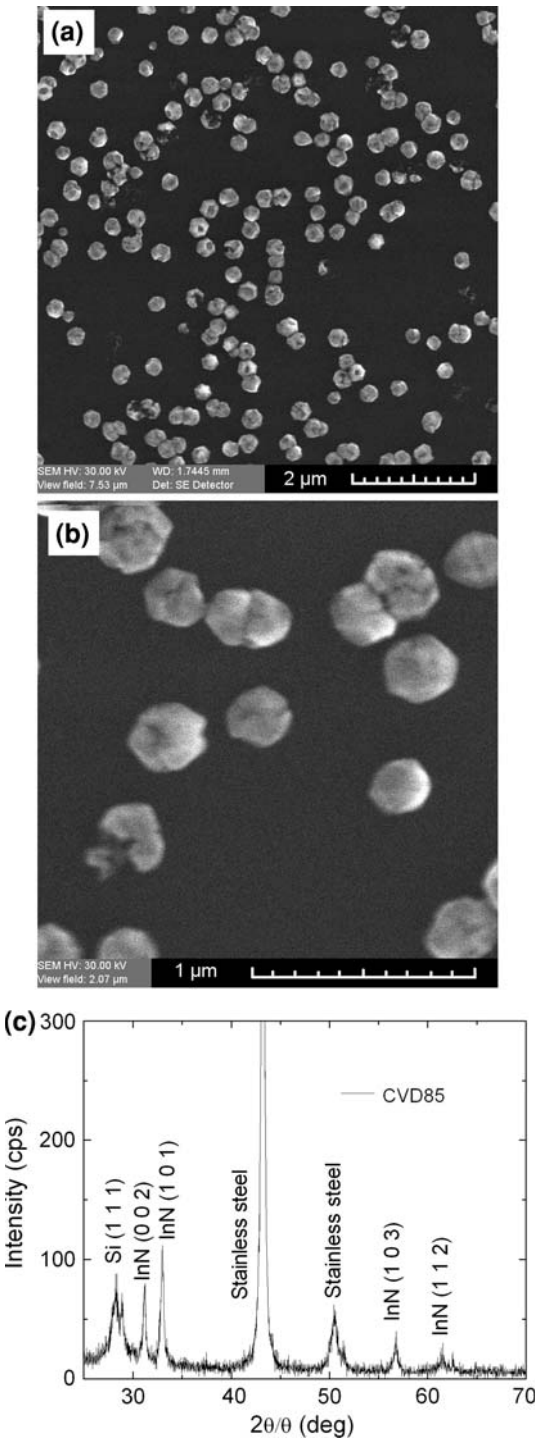


**Fig. 5** (**a**) SEM image of the InN NCs grown at 600 °C on Si(111) (**b**) high magnification of the hexagonally shaped InN NCs with diameters 200–300 nm (**c**) XRD spectrum corresponding to single phase hexagonal InN

case, when Al is heated up in a flow of $N_2$:$NH_3$ it leads to the formation of AlN around the source of Al which in turn inhibits the transfer of Al into the gas stream and consequently the growth of AlN. At high temperatures the molten Al expands and breaks the surrounding AlN shell thereby releasing Al. After cool down the residual Al appears to have expanded and has a porous like appearance. The formation of AlN on the Al source has been shown to be inhibited by incorporating $NH_4Cl$ in the Al. The decomposition of $NH_4Cl$ enhances the porosity of the Al melt thereby promoting the transfer of Al into the gas stream. On the other hand, the reaction of $NH_4Cl$ and Al leads to the formation of $AlCl_3$ which is a gas and this reacts in turn with nitrogen giving AlN according to,

$$NH_4Cl_{(S)} \longrightarrow NH_3 + HCl \tag{1}$$

$$Al + 3HCl \longrightarrow AlCl_3 + \frac{3}{2}H_2 \tag{2}$$

$$AlCl_3 + \frac{1}{2}N_2 + \frac{3}{2}H_2 \longrightarrow AlN + 3HCl. \tag{3}$$

In the case of In, we find that incorporation of $NH_4Cl$ leads to the complete transfer of the solids of In and $NH_4Cl$ into the gas stream of $N_2$. Indium has a low melting point of 156 °C and once molten it forms a sphere whose size depends on the initial amount of powder. The complete elimination of the In and $NH_4Cl$ is a direct consequence of the sublimation of the $NH_4Cl$ into $NH_3$ and HCl which occurs at 338 °C. According to Chaiken et al. [32], the sublimation rate of $NH_4Cl$ increases by a factor of $10^4$ when changing the temperature from $T = 100$–600 °C and the typical sublimation weight loss of $NH_4Cl$ is over 90% when heated for ≈60 min. Sublimation is endothermic and the temperature is expected to be reduced only by a few tens °C in the case of $NH_4Cl$ [32].

Consequently, the sublimation of $NH_4Cl$ enhances the porosity of the In resulting into an efficient transfer of In from the interior of the melt into the gas stream where it subsequently reacts with the HCl thereby forming InCl, $InCl_2$ and $InCl_3$. However, gaseous $InCl_3$ at temperatures >400 °C suffers decomposition and yields InCl and $InCl_2$ while the amount of InCl increases with increasing temperature [33]. Thus, during growth for $T > 400$ °C $InCl_3$ decomposes predominantly into InCl according to,

$$InCl_3 \rightarrow InCl + Cl_2. \tag{4}$$

InCl is yellow, changes to red at 120 °C and has a relatively low melting point of 216 °C. The InCl molecules adsorb on the Si(111) surface and react with $H_2O$ possibly absorbed by the $NH_4Cl$ to form $In_2O_3$ NCs according to,

$$2InCl + 3H_2O \rightarrow In_2O_3 + 2HCl + 2H_2. \tag{5}$$

A similar reaction involving spraying of $InCl_3$. $H_2O$ in ethanol was recently employed for the deposition of a polycrystalline thin film of $In_2O_3$ on stripe-patterned Si at 280 °C [34].

The $In_2O_3$ NCs have a stable, light yellow colour, even after exposure to the ambient air. However, most of the InCl is carried downstream as evidenced by the large amounts of dark yellow powder found only near the cool end of the reactor. Both InCl and $InCl_2$ decompose into In and Cl when reacting with $H_2O$ and so lead to the separation of metallic indium. Therefore, the rapid change of the dark yellow powder to metallic grey upon exposure to the ambient air is attributed to the humidity of the air, i.e. $H_2O$. It is important to point out that the $In_2O_3$ NCs were also obtained via the sublimation of $NH_4Cl$ in In under the presence of $O_2$ for $T < 900$ °C. In contrast, no $In_2O_3$ NCs were obtained in the case of the oxidation of In alone by $O_2$ for $T < 900$ °C. The formation of $In_2O_3$ pyramidal NCs on Si(111) was confirmed by the XRD spectrum shown in Fig. 2. In both XRD spectra illustrated in Fig. 2, only the $In_2O_3$ reflections are observed ensuring the absence of a second phase. All $In_2O_3$ peaks in Fig. 2 correspond to the $In_2O_3$ peaks also observed by Du et al. [35] who have grown $In_2O_3$ structures by dehydration of $In(OH)_3$ after heat treatment at 500 °C for 4 h. The $In_2O_3$ peaks have higher intensities for growth temperatures above 600 °C.

On the other hand, the sublimation of $NH_4Cl$ in the In under a gas flow of $NH_3$ does not yield pyramidal NCs. Upon carrying out the reaction of In with $NH_4Cl$ in a gas flow of 250 sccm of $NH_3$ as opposed to $N_2$ at 600 °C [31] we obtained single phase, hexagonal structured InN NPs with an average diameter of 300 nm as shown in Fig. 5b and confirmed by XRD shown in Fig. 5c where the (002), (101), (103) and (112) reflections of the InN, Si (111) and the stainless steel holder peaks are observed. In this case the InCl reacts with the $NH_3$ giving InN similar to the recent investigation of Kumagai et al. [36] on hydride vapour phase epitaxy of InN epitaxial layers via the reaction of $InCl_3$ with $NH_3$. These InN NCs are also very similar in size and morphology with those obtained by MOCVD on GaN [2].

An interesting aspect of the $In_2O_3$ NCs obtained from the reaction of In with $NH_4Cl$ is that they self-assemble into well-defined circles for $T \leq 600$ °C, as shown in Fig. 6a and coalesce near the periphery leading to the formation of μm size, flower-like structures, as shown in Fig. 6b at $T = 500$ °C resembling a wreath. Upon reducing the temperature to 400 °C we do not find anymore isolated $In_2O_3$ NCs but only μm size flower-like structures which now fill the wreaths, as shown in Fig. 6c. This type of self-assembly was not observed for the $In_2O_3$ NCs grown by direct oxidation of In with $O_2$ at $T > 900$ °C which aggregate into dendrites that consist of NC-chains. A possible explanation for this type of self-assembly is wetting of the Si(111) surface by In. The wetting is not uniform across the sample but instead the In forms wet circular regions on the Si(111) surface which tend to

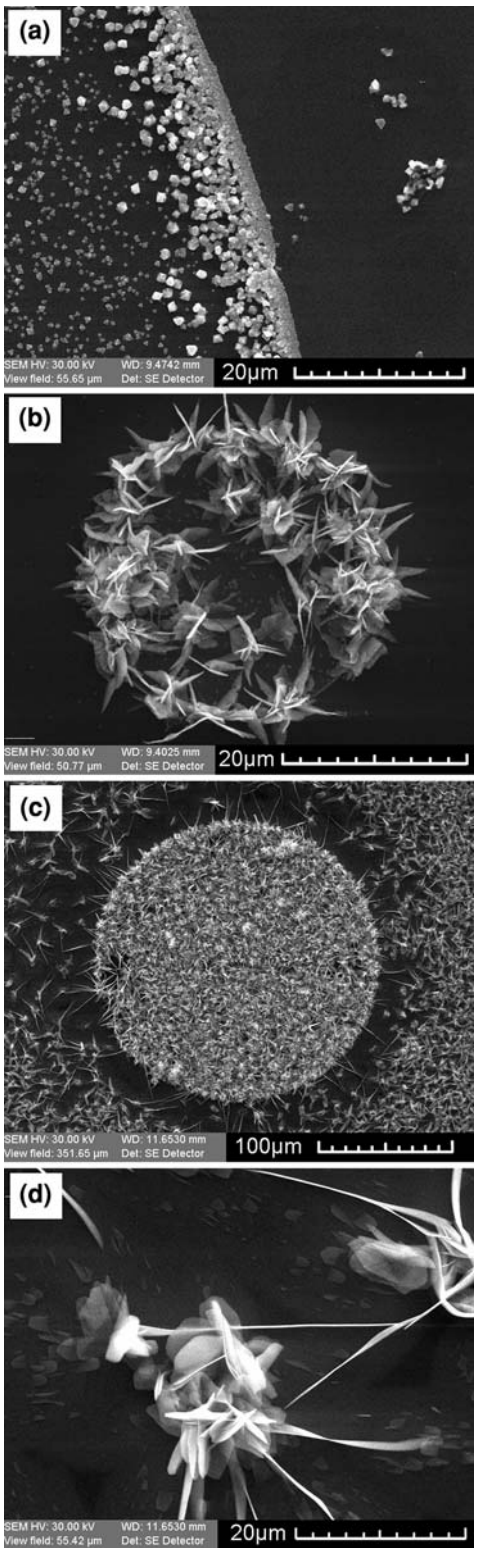


**Fig. 6** **a** Coalescence of $In_2O_3$ NCs at the periphery of a well-defined circle and formation of flower-like structures **b** Coalescence of $In_2O_3$ NCs into 'flowers' and formation of a wreath spanning over 20 μm, obtained at $T_G = 500$ °C **c** Large wreath full of flower-like structures spanning over almost 200 μm obtained at $T_G = 400$ °C and **d** 20 μm isolated flower-like structure

expand as the growth proceeds thereby leading to the coalescence of the NCs and the formation of the wreath-like structures shown in Fig. 6a–d. These wreath-like structures become larger when decreasing the temperature and the individual flower-like structures may grow up to 20 μm, Fig. 6d.

## Conclusion

We have investigated the synthesis of $In_2O_3$ NCs by direct oxidation of In with $O_2$ and also by the incorporation of $NH_4Cl$ in the In under $N_2$. The reaction of In and $NH_4Cl$ yields InN NCs using $NH_3$. The synthesis of $In_2O_3$ NCs by direct oxidation of In with $O_2$ is limited by the formation of an oxide shell surrounding the In which can be eliminated only at $T_G > 900$ °C as a consequence of the expanding melt therefore allowing an efficient transfer of In into the main gas stream. At $T_G > 1000$ °C we obtain 500 nm size $In_2O_3$ NCs but also dendrite structures consisting of NC chains.

The high temperature requirement can be alleviated by the addition of $NH_4Cl$ into the In which breaks down into $NH_3$ and HCl by sublimation thus resulting into the complete transfer of the In into the gas stream and the formation of InCl which reacts with $H_2O$ and $O_2$. In this way we obtained $In_2O_3$ NCs at temperatures as low as 500 °C under $N_2$ but also InN by simply changing from $N_2$ to $NH_3$. This method is potentially interesting for the synthesis of narrow and wide-band gap InN and $In_2O_3$ NCs at low temperatures but also for nano-engineering of heterostructures and the fabrication of novel devices such as third generation solar cells.

## References


1. J.G. Lozano, A.M. Sánchez, R. García, S. Ruffenach, O. Briot, D. González, Nanoscale Res. Lett. **2**, 442 (2007). doi:10.1007/s11671-007-9080-6
2. O. Briot, B. Maleyre, S. Ruffenach, Appl. Phys. Lett. **83**, 2919 (2003). doi:10.1063/1.1613044
3. T. Yoshida, S. Takeyama, Y. Yamada, K. Mutoh, Appl. Phys. Lett. **68**, 68 (1996). doi:10.1063/1.116662
4. X.D. Pi, R. Gresback, R.W. Liptak, S.A. Campbell, U. Kortshagen, Appl. Phys. Lett. **92**, 123102 (2008). doi:10.1063/1.2897291
5. J.P. Wilcoxon, P.P. Provencio, G.A. Samara, Phys. Rev. B **64**, 035417 (2001). doi:10.1103/PhysRevB.64.035417
6. J. Perrière, E. Millon, M. Chamarro, M. Morcrette, C. Andreazza, Appl. Phys. Lett. **78**, 2949 (2001). doi:10.1063/1.1370992
7. S. Wei, J. Lu, W. Yu, Y. Qian, J. Appl. Phys. **95**, 3683 (2004). doi:10.1063/1.1650883
8. D. Bertram, O.I. Mićić, A.J. Nozik, Phys. Rev. B **57**, R4265 (1998). doi:10.1103/PhysRevB.57.R4265
9. M.R. Greenberg, W. Chen, B.N. Pulford, G.A. Smolyakov, J.S. Ying-Bing, D. Bunge, T.J. Boyle, Proc SPIE **5705**, 68 (2005). doi:10.1117/12.601507
10. O.I. Mićić, S.P. Ahrenkiel, D. Bertram, A.J. Nozik, Appl. Phys. Lett. **75**, 478 (1999). doi:10.1063/1.124414
11. R.B. Little, M.A. El-Sayed, G.W. Bryant, S. Burke, J. Chem. Phys. **114**, 1813 (2001). doi:10.1063/1.1333758
12. D.R. Jung, D. Son, J. Kim, C. Kim, B. Park, Appl. Phys. Lett. **93**, 163118 (2008). doi:10.1063/1.3007980
13. N.V. Hullavarad, S.S. Hullavarad, J. Vac. Sci. Technol. A **26**, 1050 (2008). doi:10.1116/1.2940346
14. M. Ghosh, A.K. Raychaudhuri, J. Appl. Phys. **100**, 034315 (2006). doi:10.1063/1.2227708
15. L.B. Duan, G.H. Rao, J. Yu, Y.C. Wang, W.G. Chu, L.N. Zhang, J. Appl. Phys. **102**, 103907 (2007). doi:10.1063/1.2815647
16. M. Snure, A. Tiwari, J. Appl. Phys. **104**, 073707 (2008). doi:10.1063/1.2988131
17. W.Q. Peng, S.C. Qu, G.W. Cong, Z.G. Wang, Appl. Phys. Lett. **88**, 101902 (2006). doi:10.1063/1.2182010
18. N. Shirahata, A. Hozumi, A. Asakura, A. Fuwa, Y. Sakka, J. Vac. Sci. Technol. A **23**(4), 731 (2005). doi:10.1116/1.1863936
19. H. Jia, Y. Zhang, X. Chen, J. Shu, X. Luo, Z. Zhang, Appl. Phys. Lett. **82**, 4146 (2003). doi:10.1063/1.1582354
20. G. Cheng, E. Stern, S. Guthrie, M.A. Reed, R. Klie, Y. Hao, G. Meng, L. Zhang, Appl. Phys. **A85**, 233 (2006)
21. P. Guha, S. Kar, S. Chaudhuri, Appl. Phys. Lett. **85**, 3851 (2004). doi:10.1063/1.1808886
22. H. Zhou, W. Cai, L. Zhang, Appl. Phys. Lett. **75**, 495 (1999). doi:10.1063/1.124427
23. M. Wei, D. Zhi, J.L. MacManus-Driscoll, Nanotechnology **17**, 3523 (2006). doi:10.1088/0957-4484/17/14/027
24. J. Ederth, P. Johnsson, G.A. Niklasson, A. Hoel, A. Hultåker, P. Heszler, C.G. Granqvist, A.R. van Doorn, M.J. Jongerius, Phys. Rev. B **68**, 155410 (2003). doi:10.1103/PhysRevB.68.155410
25. T.S. Ko, C.P. Chu, J.R. Chen, Y.A. Chang, T.C. Lu, H.C. Kuo, S.C. Wang, J. Vac. Sci. Technol. A **25**, 1038 (2007)
26. A. Murali, A. Barve, V.J. Leppert, S.H. Risbud, I.M. Kennedy, H.W.H. Lee, Nano. Lett. **1**, 287 (2001). doi:10.1021/nl010013q
27. P. Zhu, W. Wu, J. Zhou, W. Zhang, Appl. Organomet. Chem. **21**, 909 (2007). doi:10.1002/aoc.1300
28. G.Q. Ding, W.Z. Chen, M.J. Zheng, Z.B. Zhou, Appl. Phys. Lett. **89**, 063113 (2006). doi:10.1063/1.2335665
29. X.-J. Huang, Y.-K. Choi, Sens Actuators **B122**, 659 (2007)
30. J. T-Thienprasert, J. Nukeaw, A. Sungthong, S. Porntheeraphat, S. Singkarat, D. Onkaw, S. Rujirawat, S. Limpijumnong, Appl. Phys. Lett. **93**, 0519031 (2008). doi:10.1063/1.2965802
31. A. Othonos, M. Zervos, M. Pervolaraki, Nanoscale Res. Lett. **4**, 122 (2009)
32. R.F. Chaiken, D.J. Sibbett, J. Sutherland, D.K. Van de Mark, A. Wheeler, J. Chem. Phys. **37**, 2311 (1962). doi:10.1063/1.1733003
33. A. Haaland, *The Molecular Structures of Main Group Element Compounds*, Chap. 11, Oxford University Press US (2008), ISBN 019923535X, 9780199235353
34. T. Kondo, H. Funakubo, K. Akiyama, H. Enta, Y. Seki, M.H. Wang, T. Uchida, Y. Sawada, J. Cryst. Growth (2008) (in press)
35. J. Du, M. Yang, S.N. Cha, D. Rhen, M. Kang, D.J. Kang, Cryst. Growth Des. **8**, 2312 (2008). doi:10.1021/cg701058v
36. Y. Kumagai, J. Kikuchi, Y. Nishizawa, H. Murakami, A. Koukitu, J. Cryst. Growth **300**, 57 (2007). doi:10.1016/j.jcrysgro.2006.10.202